Plasmonic terahertz lasing in an array of graphene nanocavities

V. V. Popov,[1,2,*] O. V. Polischuk,[1,2] A. R. Davoyan,[1] V. Ryzhii,[3] T. Otsuji,[3] and M. S. Shur[4]

[1]*Kotelnikov Institute of Radio Engineering and Electronics (Saratov Branch), Russian Academy of Sciences, Saratov 410019, Russia*

[2]*Saratov State University, Saratov 410012, Russia*

[3]*Research Institute for Electrical Communication, Tohoku University, Sendai 980-8577, Japan*

[4]*Department of Electrical, Computer, and Systems Engineering, Rensselaer Polytechnic Institute, Troy, New York 12180, USA*

(Received 27 July 2012; revised manuscript received 31 October 2012; published 30 November 2012)

We propose a novel concept of terahertz lasing based on stimulated generation of plasmons in a planar array of graphene resonant micro/nanocavities strongly coupled to terahertz radiation. Due to the strong plasmon confinement and superradiant nature of terahertz emission by the array of plasmonic nanocavities, the amplification of terahertz waves is enhanced by many orders of magnitude at the plasmon resonance frequencies. We show that the lasing regime is ensured by the balance between the plasmon gain and plasmon radiative damping.

DOI: 10.1103/PhysRevB.86.195437 PACS number(s): 73.20.Mf, 07.57.Hm, 78.67.Wj, 42.60.Lh

Fundamental limits reached by the available sources of electromagnetic radiation based on classical electronic oscillations radiating at radio and microwave frequencies, and on electron transitions between quantized energy levels corresponding to infrared and optical frequencies, give rise to the so-called terahertz (THz) gap.[1,2]

Extraordinary electronic properties of novel materials might help to go beyond the limits of the THz gap. In particular, graphene, a two-dimensional monolayer of graphite, has received a great deal of interest recently due to its unique electronic properties stemming from a linear (Dirac-type) gapless carrier energy spectrum $\mathcal{E} = \pm V_F|p|$ (see the inset in Fig. 1), where $\mathcal{E}$ and p are the electron (hole) energy and momentum, respectively, $V_F \approx 10^8$ cm/s is the Fermi velocity, which is a constant for graphene, and upper and lower signs refer to the conduction and valence bands, respectively.[3,4] Graphene is especially promising for THz photonics[5] due to its zero (or small in doped graphene) band gap.

Interband population inversion in graphene can be achieved by its optical pumping[6] or carrier injection.[7] At sufficiently strong excitation, the interband stimulated emission of photons can prevail over the intraband (Drude) absorption. In this case, the real part of the dynamic conductivity of graphene can be negative in the THz range. This effect can be used for THz photon lasing.[8] Stimulated emission of near-infrared[9] and THz[10] photons from population inverted graphene was recently observed.

Graphene exhibits strong plasmonic response due to both high density and small "relativistic" effective mass $m_F = \mathcal{E}_F/V_F^2$ of free carriers, where $\mathcal{E}_F$ is the Fermi energy. Dispersion of the plasma waves (plasmons) in graphene was studied for intrinsic (undoped)[11,12] and doped (or gated)[13–17] graphene. Plasmon resonances in graphene can be controlled in graphene nanoribbon arrays[18–20] and tuned in the entire THz range, depending on the direction of the plasmon propagation in the array plane and/or by varying the nanoribbon width. Plasmons in patterned graphene strongly couple to electromagnetic waves, which makes graphene nanostructures very promising for the development of tunable graphene-based THz plasmonic metamaterials.[19,21–24]

Compared with the stimulated emission of electromagnetic modes (photons), the stimulated emission of plasmons by the interband transitions in population inverted graphene exhibits a much higher gain due to a small group velocity of the plasmons in graphene and strong confinement of the plasmon field in the vicinity of the graphene layer.[25,26] Plasmon emission due to recombination of the electron-hole pairs in graphene was demonstrated experimentally recently.[27] However, a large plasmon gain in graphene leads to strong dephasing of the plasmon mode, hence preventing THz lasing. Also, strong coupling between the plasmons in graphene and electromagnetic radiation can hinder THz lasing from nonequilibrium plasmons. Therefore, to the best of our knowledge, neither plasmonic amplification of THz radiation nor THz plasmonic lasing in graphene has been reported so far.

In this paper, we consider the amplification of a THz wave by the stimulated generation of resonant plasmons in a planar periodic array of graphene plasmonic micro/nanocavities strongly coupled to THz radiation. We show that, due to the strong confinement of the plasmon modes in the graphene micro/nanocavities and superradiant nature of electromagnetic emission from the array of the plasmonic micro/nanocavities, the amplification of THz waves is enhanced by several orders of magnitude at the plasmon resonance frequencies. It is shown that the plasmonic THz lasing becomes possible due to restoring the plasmon coherence in the graphene nanocavities strongly coupled to THz radiation at the balance between the plasmon gain and plasmon radiative damping.

Let us suppose that graphene micro/nanocavities are confined between the contacts of the metal grating located on a plane surface of a dielectric substrate, which can be high resistivity Si or SiC (see Fig. 1). We assume that the graphene is pumped either by optical illumination or by injection of electrons and holes from opposite metal contacts in each graphene nanocavity. In this case, the electron and hole densities in graphene can substantially exceed their equilibrium values and the electron and hole systems can be characterized by the quasi-Fermi energies $\pm\mathcal{E}_F$, respectively (see the inset in Fig. 1) and the effective temperature T. If the characteristic time of the emission of the optical phonon by an electron or a hole is much shorter than the time of the pair collisions, the nonequilibrium electrons and holes emit a cascade of optical phonons and occupy low energy states in the conduction and valence bands, respectively.

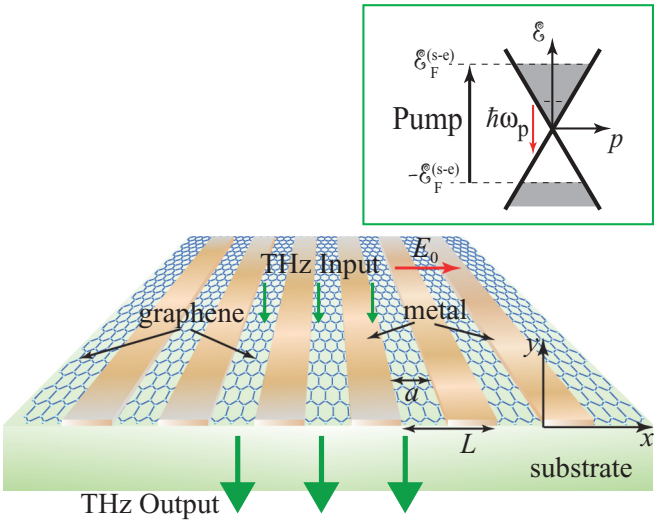

FIG. 1. (Color online) Schematic view of the array of graphene micro/nanocavities. The incoming electromagnetic wave is incident from the top at normal direction to the structure plane with the polarization of the electric field across the metal grating contacts. The energy band structure of pumped graphene is shown schematically in the inset.

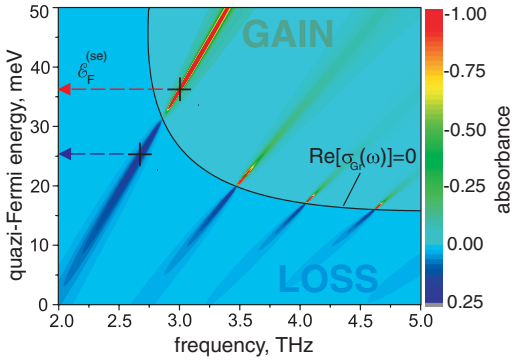

FIG. 2. (Color online) Contour map of the absorbance as a function of the quasi-Fermi energy and the frequency of incoming THz wave for the array of graphene microcavities with period $L = 4\ \mu$m and the length of a graphene microcavity $a = 2\ \mu$m. The electron scattering time in graphene is $\tau = 10^{-12}$ s. Blue and red arrows mark the quasi-Fermi energies for the maximal absorption and for the plasmonic lasing regime, respectively, at the fundamental plasmon resonance.

In this case, the contribution of nonequilibrium carriers to the heating of the electron-hole system is small and their effective temperature T is close to the lattice temperature T_0.[28] (If the effective temperature exceeds T_0, somewhat stronger pumping might be needed to ensure the population inversion in graphene.[28]) For $T = T_0$, one can describe the response of pumped graphene by its complex-valued sheet conductivity in the local approximation[26] (see also Refs. 17 and 29, as well as the recent review paper 30)

$$\sigma_{Gr}(\omega) = \left(\frac{e^2}{4\hbar}\right)\left\{\frac{8k_BT\tau}{\pi\hbar(1-i\omega\tau)}\ln\left[1+\exp\left(\frac{\mathcal{E}_F}{k_BT}\right)\right] + \tanh\left(\frac{\hbar\omega-2\mathcal{E}_F}{4k_BT}\right) - \frac{4\hbar\omega}{i\pi} \times \int_0^\infty \frac{G(\mathcal{E},\mathcal{E}_F)-G(\hbar\omega/2,\mathcal{E}_F)}{(\hbar\omega)^2-4\mathcal{E}^2}d\mathcal{E}\right\}. \quad (1)$$

Here ω is the frequency of the incoming electromagnetic wave, e is the electron charge, $\hbar$ is the reduced Planck constant, k_B is the Boltzmann constant, and

$$G(\mathcal{E},\mathcal{E}') = \frac{\sinh(\mathcal{E}/k_BT)}{\cosh(\mathcal{E}/k_BT)+\cosh(\mathcal{E}'/k_BT)}.$$

The first term in the curly braces in Eq. (1) describes a Drude-model response for the intraband processes involving the phenomenological electron and hole scattering time τ, which can be estimated from the measured dc carrier mobility: $\tau = \mu\mathcal{E}_F/eV_F^2$.[31] The temperature-independent carrier mobility $\mu > 250000\ \mathrm{cm}^2/\mathrm{V\,s}$ observed recently in multilayer epitaxial graphene on 4H-SiC substrate[32,33] corresponds to $\tau \approx 10^{-12}$ s for $\mathcal{E}_F = 40$ meV at room temperature. Carrier scattering times longer than 1 ps were observed recently by the Raman spectroscopy of optically pumped graphene[34,35] in a quasiequilibrium regime (after the carriers are equilibrated due to fast carrier-carrier scattering). The remaining terms in Eq. (1) arise from the interband transitions. For sufficiently strong degeneracy of the electron and hole systems, the quasi-Fermi energy $\mathcal{E}_F$ depends on the electron (hole) density, $N_{n(p)}(N_n = N_p)$, in graphene: $\mathcal{E}_F \sim \hbar V_F\sqrt{\pi N_{n(p)}}$.[4] Hence, the quasi-Fermi energy is determined by the photogeneration rate[36] or by the carrier injection rate[7] under optical or carrier injection pumping, respectively. Of course, the simple estimates of the phenomenological parameters given above are to be considered only as rough approximations. Their exact values are to be measured[34,35] or calculated by using a microscopic *ab initio* approach.[37–39]

We assume that the external THz electromagnetic wave is incident upon the planar array of graphene micro/nanocavities at normal direction to its plane with the polarization of the electric field across the metal grating contacts as shown in Fig. 1. Then we solve the problem of the amplification of the THz wave by the array of graphene micro/nanocavities in a semianalytical self-consistent electromagnetic approach similar to that described in Ref. 40 (for more details of our theoretical approach see Ref. 41).

Figure 2 shows the contour map of the calculated absorbance as a function of the quasi-Fermi energy (which corresponds to the pumping strength) and the THz wave frequency for an array of the graphene microcavities with period $L = 4\ \mu$m and the length of each microcavity $a = 2\ \mu$m. The absorbance is defined as the ratio between the absorbed or emitted (which corresponds to negative absorbance) THz power per unit area of the array and the energy flux density in the incoming THz wave. In the amplification regime, the negative value of the absorbance yields the amplification coefficient. The value of Re$[\sigma_{Gr}(\omega)]$ is negative above the solid black line in Fig. 2, corresponding to Re$[\sigma_{Gr}(\omega)] = 0$ (i.e., to transparent graphene). Above this boundary line, negative absorption (i.e., amplification) takes place at all frequencies and pumping strengths. The plasmon absorption resonances below the Re$[\sigma_{Gr}(\omega)] = 0$ line give way to the amplification resonances above this line. Plasmon resonances appear at

frequencies $\omega = \omega_p(q)$ determined by the selection rule for the plasmon wave vector $q_n = (2n-1)\pi/a_{\text{eff}}$, where a_{eff} is the effective length of the graphene micro/nanocavity. The effective length of the graphene micro/nanocavity can be, in general, different from its geometric length a due to the effect of the metal contacts (see the related discussion for a conventional two-dimensional electron system in Ref. 42). The frequency of the plasmon resonance is determined mainly by the imaginary part of the graphene conductivity in Eq. (1), while the real part of the conductivity is responsible for the energy loss (for $\text{Re}[\sigma_{Gr}(\omega)] > 0$) or energy gain (for $\text{Re}[\sigma_{Gr}(\omega)] < 0$).

As seen from Fig. 2, the absorbance (including the negative absorbance in the amplification regime) at the plasmon resonance does not vary monotonously with increasing $\mathcal{E}_F$, but rather exhibits absorption and amplification maxima at some values of the quasi-Fermi energy. The reason is that the absorbed or amplified electromagnetic power depends not only on the plasmon loss due to its energy dissipation, $\gamma_{\text{dis}}(\mathcal{E}_F,\omega) < 0$, or plasmon gain, $g(\mathcal{E}_F,\omega) > 0$, respectively, but also on the coupling between the plasmons and electromagnetic wave. Coupling might be different for different structures but, basically, it is controlled by the radiative damping, $\gamma_{\text{rad}}(\mathcal{E}_F,\omega)$, due to plasmon radiative decay into electromagnetic waves. General phenomenological consideration of THz absorption in a planar periodic plasmonic structure[43–45] shows that the maximal absorption at the plasmon resonance takes place when $\gamma_{\text{dis}} = \gamma_{\text{rad}}$ irrespective of details of the plasmonic structure.

For zero pumping strength, the dissipative damping of the plasmons in graphene, γ_{dis}, comes from the energy loss due to the electron and hole scattering with the decay rate γ_{sc} and the energy loss due to generation of the electron-hole pairs with the decay rate $\gamma_{e\text{-}h}$. Hence $\gamma_{\text{dis}} = \gamma_{sc} + \gamma_{e\text{-}h}$. These two different energy loss mechanisms are accounted for by the first and second terms in the curly braces in Eq. (1), respectively. In the structure under consideration, the dissipative broadening of the plasmon resonance resulting from the carrier scattering in graphene for $\tau = 10^{-12}$ s is $2\gamma_{sc} = 1/2\pi\tau \approx 0.16$ THz. The plasmon loss resulting from the generation of the electron-hole pairs by the THz wave depends on frequency, see Eq. (1), and leads to a plasmon resonance broadening of about 0.014 THz at frequency 1.96 THz of the fundamental plasmon resonance in Fig. 2 for zero pumping strength, $\mathcal{E}_F = 0$. The radiative broadening of the plasmon resonance depends on both the carrier concentration in graphene and on the antenna properties of the planar periodic plasmonic structure.[43–45] In the "cold" structure (without pumping), the radiative broadening of the first plasmon resonance in Fig. 2 is about 0.01 THz.

For $2\mathcal{E}_F > \hbar\omega$, the energy loss due to the generation of the electron-hole pairs described by the second term in the curly braces in Eq. (1) becomes negative (which corresponds to the energy gain), while the net loss can be still positive due to the electron (hole) scattering contribution, so that the plasmon net dissipative damping becomes smaller. Because the electron scattering loss in graphene for $\mathcal{E}_F = 0$ is typically greater than the plasmon radiative loss in the array of the graphene micro/nanocavities, the plasmon net dissipative damping becomes equal to their radiative damping at some pumping strength $\mathcal{E}_F > 0$ that results in the maximal absorption at the plasmon resonance. The quasi-Fermi energy

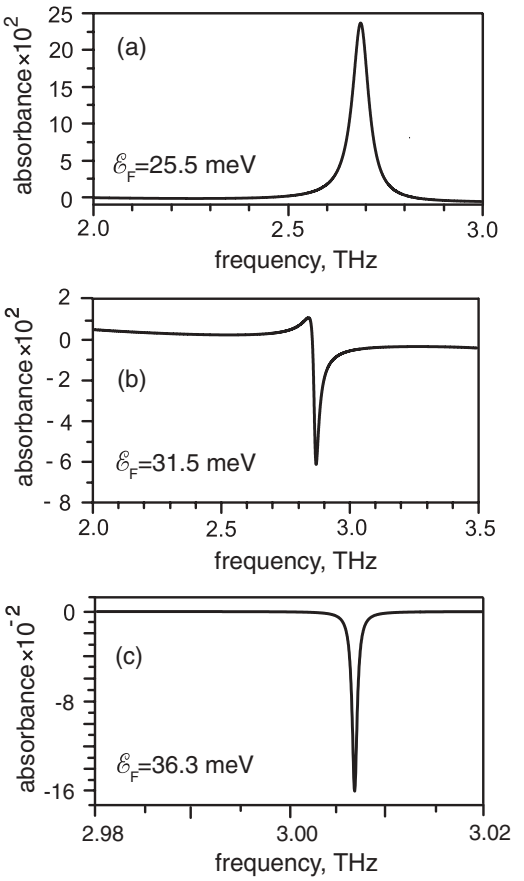

FIG. 3. The fundamental plasmon resonance (a) in the maximal absorption regime, (b) near the graphene transparency regime $\text{Re}[\sigma_{Gr}(\omega)] = 0$, and (c) near the self-excitation regime.

value corresponding to the maximal absorption at the first plasmon resonance is marked by the blue arrow in Fig. 2. The maximal theoretical value of the absorbance at the plasmon resonance is[44,45] $A_{\text{res}}^{\max} = 0.5(1 - \sqrt{R_0})$, where R_0 is the reflectivity of a bare substrate, which yields $A_{\text{res}}^{\max} \approx 0.23$ for a silicon substrate [see Fig. 3(a)].

With further increase of $\mathcal{E}_F$, the energy gain can balance the energy loss caused by the electron scattering in graphene resulting in zero net energy loss, $\text{Re}[\sigma_{Gr}(\omega)] = 0$, and corresponding graphene transparency. In this case, the plasmon resonance line exhibits a nonsymmetric Fano-like shape[46,47] shown in Fig. 3(b), since the real part of graphene conductivity changes sign across the plasmon resonance. The linewidth of the Fano-like plasmon resonance is given mainly by its radiative broadening (since the dissipative damping is close to zero in this case). The radiative linewidth of the Fano-like resonance at $\text{Re}[\sigma_{Gr}(\omega)] = 0$ is greater than that for zero pumping ($\mathcal{E}_F = 0$) because the carrier density in graphene is higher for $\mathcal{E}_F > 0$.

Above the graphene transparency line $\text{Re}[\sigma_{Gr}(\omega)] = 0$, the THz wave amplification at the plasmon resonance frequency [see Fig. 3(c)] is several orders of magnitude stronger than away from the resonances (the latter corresponding to the photon amplification in population inverted graphene[9,10]). Note that at a certain value of the quasi-Femi energy, $\mathcal{E}_F = \mathcal{E}_F^{(se)}$, the amplification coefficient at the plasmon resonance tends

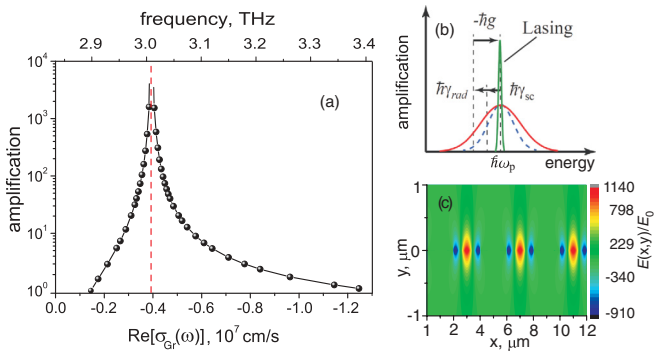

FIG. 4. (Color online) (a) The variation of the power amplification coefficient along the first-plasmon-resonance lobe (see Fig. 2) near the self-excitation regime. The frequency of the plasmon lasing is marked by the vertical dashed line. (b) Schematic illustration of the energy rate balance in the plasmon lasing regime. (c) The snapshot of the distribution of the normalized induced in-plane electric field at the moment of time corresponding to the maximal swing of plasma oscillations in the graphene microcavities at the fundamental plasmon amplification resonance shown in Fig. 3(c).

toward infinity with corresponding amplification linewidth shrinking down to zero. This corresponds to plasmonic lasing in the graphene micro/nanocavities in the self-excitation regime. The behavior of the amplification coefficient around the self-excitation regime is shown in Fig. 4(a). The lasing occurs when the plasmon gain balances the electron scattering loss and the radiative loss, $g(\mathcal{E}_F^{(se)},\omega) = -[\gamma_{\rm rad}(\mathcal{E}_F^{(se)},\omega) + \gamma_{sc}]$; see Fig. 4(b). It means that the plasmon oscillations are highly coherent in this case, with virtually no dephasing at all. When $g(\mathcal{E}_F,\omega) < -[\gamma_{\rm rad}(\mathcal{E}_F^{(se)},\omega) + \gamma_{sc}]$, a fast radiative decay hinders the plasmon stimulated generation in graphene, whereas when $g(\mathcal{E}_F,\omega) > -[\gamma_{\rm rad}(\mathcal{E}_F^{(se)},\omega) + \gamma_{sc}]$ a low radiative decay rate slows down the release of the plasmon energy into THz radiation. The quasi-Fermi energy corresponding to plasmonic lasing in the first plasmon resonance is marked by the red arrow in Fig. 2. Weaker plasmon gain is needed to meet the self-excitation condition at the higher-order plasmon resonances because of smaller radiative damping (due to a smaller oscillator strength) of the higher-order plasmon modes. Hence, plasmonic lasing takes place at quasi-Fermi energy values closer to the graphene-transparency line $\mathrm{Re}[\sigma_{Gr}(\omega)] = 0$ for the higher-order plasmon resonances (see Fig. 2). Therefore, dynamic and frequency ranges of plasmonic lasing decrease for higher order resonances. Plasmon radiative damping not only determines the plasmonic lasing condition, but also plays a constructive role in the amplification process. By conservation of energy, the electromagnetic power emitted from the array of graphene micro/nanocavities is proportional to the radiative decay rate of stored energy, $2|\gamma_{\rm rad}|$. Hence, a much higher amplification coefficient can be reached at the first plasmon resonance as compared to that for the higher-order plasmon resonances (in the same frequency range around the self-excitation frequency).

Of course, the divergence of the amplification coefficient at $\mathcal{E}_F = \mathcal{E}_F^{(se)}$ is unphysical. It is a consequence of the linear electromagnetic approach used in this work. It is natural to assume that the linear approach is quantitatively valid when the amplitude of amplified plasmon oscillations in graphene is much smaller than the unperturbed density of the photogenerated or injected electron-hole pairs. Estimating the unperturbed density of the nonequilibrium carriers as $(N_n + N_p) \sim 2\mathcal{E}_F^2/(\pi\hbar^2 V_F^2) \approx 4 \times 10^{11}$ cm^{-2} for $\mathcal{E}_F =$ 36 meV, we can claim that our approach is quantitatively valid up to power amplification coefficients of 10^3 or even higher. (For example, the fluctuations corresponding to blackbody radiation at 300 K would be amplified above the mW/cm^2 level at the plasmon resonance frequencies.) This value of the amplification coefficient is five orders of magnitude higher than that away from the plasmon resonance. We expect that the main conclusions of this paper concerning general properties and conditions of the amplification process and plasmon lasing remain valid qualitatively even for greater amplification coefficients.

Although we presented the above results of numerical calculations obtained for an array of graphene microcavities, similar results were obtained also for an array of graphene nanocavities. The plasmon resonance frequency is roughly proportional to the inverse value of the square root of the nanocavity length, so that, for example, the lasing at the fundamental plasmon resonance takes place at a frequency of about 6.7 THz at $\mathcal{E}_F = 18$ meV for the graphene nanocavity length 200 nm. It is worth mentioning that the main results of our paper remain valid also for a shorter relaxation time. Only the corresponding values of the quasi-Fermi energy and the frequency of the plasmonic lasing increase somewhat in this case. For example, assuming the carrier relaxation time 0.1 ps, we obtain the plasmonic lasing at frequency 9.8 THz of the fundamental plasmon resonance for a quasi-Fermi energy value of about 55 meV in an array of the graphene nanocavities of length 200 nm each.

Enhanced THz emission from the graphene nanocavities is caused by the fact that plasmons in different nanocavities oscillate in phase (even without the incoming electromagnetic wave) because the metal contacts act as synchronizing elements between adjacent graphene nanocavities (applying a mechanical analogy, one may think of rigid crossbars connecting oscillating springs arranged in a chain). Therefore, the plasma oscillations in the array of graphene nanocavities constitute a single collective plasmon mode distributed over the entire area of the array, which leads to the enhanced superradiant electromagnetic emission from the array. The plasmon-mode locking regime among different graphene nanocavities is illustrated in Fig. 4(c). Extraordinary properties of a collective mode in an array of synchronized dipole oscillators are well known in quantum optics: the power of electromagnetic emission from such an array grows as the square of the number of the oscillators in the array.[48] Superradiant plasmon resonances in concentric ring/disc gold nanocavities in the visible and near-infrared spectral ranges were experimentally demonstrated recently.[49]

Giant THz amplification enhancement at the plasmon resonance is also ensured by strong plasmon confinement in the graphene micro/nanocavities; see Fig. 4(c). A large plasmon gain in graphene would lead to the strong dephasing of a plasma wave over quite long propagation distance (which corresponds to the nonresonant stimulated generation of plasmons[25,26]). Therefore, strong plasmon-mode confinement

in a single-mode plasmonic cavity is required to ensure the resonant stimulated generation of plasmons. Plasmon confinement to a single-mode micro/nanocavity also enhances the rate of spontaneous electromagnetic emission by the plasmon mode due to the Purcell effect.[50] It is expected that the confinement of plasmons in a two-dimensional array of graphene micro/nanocavities could enhance the amplification even more.

In conclusion, we predict a giant amplification and lasing of THz radiation due to the stimulated generation of plasmons in an array of graphene resonant micro/nanocavities strongly coupled to THz radiation. The amplification of the THz wave at the plasmon resonance frequencies is several orders of magnitude stronger than away from the resonances. Giant THz wave amplification is due to the strong plasmon confinement and superradiant nature of THz emission by the array of plasmonic micro/nanocavities. The THz lasing at the plasmon resonance is achieved when the net plasmon gain in graphene approaches the negative of the radiative damping of the resonant plasmons, which ensures high plasmon coherence and self-excitation of plasmons in the graphene nanocavities. The amplification resonance line is mainly of Lorentzian shape except when the net energy gain in graphene is close to zero. In that case, a Fano-like resonant lineshape is formed due to a strong variation of the graphene conductivity across the resonance linewidth. These results might be of broad physical interest as revealing new general features of the strong interaction of an array of nonequilibrium oscillators with electromagnetic radiation. In terms of practical applications, these results can pave a way to creation of plasmonic graphene amplifiers and generators for THz frequencies.

The work was supported by the Russian Foundation for Basic Research (Grants No. 11-02-92101 and No. 12-02-93105) and by the Russian Academy of Sciences Program "Technological Fundamentals of Nanostructures and Nanomaterials." The work at RPI was supported by the US NSF under the auspices of I/UCRC "CONNECTION ONE," NSF I-Corp, and by the NSF EAGER program. This work was financially supported in part by NPRP Grant No. NPRP 09-1211-2-475 from the Qatar National Research Fund, by the JSPS Grant-in-Aid for Specially Promoting Research (No. 23000008), Japan, by the JSPS-RFBR Japan-Russian Collaborative Research Program, and by JST-CREST, Japan.

*popov_slava@yahoo.co.uk

[1] X.-C. Zhang and J. Xu, *Introduction to THz Wave Photonics* (Springer-Verlag, New York, 2009).
[2] M. Tonouchi, Nature Photon. **1**, 97 (2007).
[3] K. S. Novoselov, A. K. Geim, S. V. Morozov, D. Jiang, Y. Zhang, S. V. Dubonos, I. V. Grigorieva, and A. A. Firsov, Science **306**, 666 (2004).
[4] A. H. Castro Neto, F. Guinea, N. M. R. Peres, K. S. Novoselov, and A. K. Geim, Rev. Mod. Phys. **81**, 109 (2009).
[5] B. Sensale-Rodriguez, R. Yan, M. M. Kelly, T. Fang, K. Tahy, W. S. Hwang, D. Jena, L. Liu, and H. G. Xing, Nature Commun. **3**, 780 (2012).
[6] A. Satou, F. T. Vasko, and V. Ryzhii, Phys. Rev. B **78**, 115431 (2008).
[7] V. Ryzhii, M. Ryzhii, V. Mitin, and T. Otsuji, J. Appl. Phys. **110**, 094503 (2011).
[8] V. Ryzhii, M. Ryzhii, A. Satou, N. Ryabova, T. Otsuji, V. Mitin, F. T. Vasko, A. A. Dubinov, V. Y. Aleshkin, and M. S. Shur, *Future Trends in Microelectronics*, edited by S. Luryi, J. Xu, and A. Zaslavsky (John Wiley & Sons, New York, 2010).
[9] T. Li, L. Luo, M. Hupalo, J. Zhang, M. C. Tringides, J. Schmalian, and J. Wang, Phys. Rev. Lett. **108**, 167401 (2012).
[10] S. Boubanga-Tombet, S. Chan, T. Watanabe, A. Satou, V. Ryzhii, and T. Otsuji, Phys. Rev. B **85**, 035443 (2012).
[11] O. Vafek, Phys. Rev. Lett. **97**, 266406 (2006).
[12] L. A. Falkovsky and A. A. Varlamov, Eur. Phys. J. B **56**, 281 (2007).
[13] V. Ryzhii, Jpn. J. Appl. Phys. **45**, L923 (2006).
[14] B. Wunsch, T. Stauber, F. Sols, and F. Guinea, New J. Phys. **8**, 318 (2006).
[15] E. H. Hwang and S. Das Sarma, Phys. Rev. B **75**, 205418 (2007).
[16] V. Ryzhii, A. Satou, and T. Otsuji, J. Appl. Phys. **101**, 024509 (2007).
[17] G. W. Hanson, J. Appl. Phys. **103**, 064302 (2008).
[18] V. V. Popov, T. Y. Bagaeva, T. Otsuji, and V. Ryzhii, Phys. Rev. B **81**, 073404 (2010).
[19] L. Ju, B. Geng, J. Horng, C. Girit, M. Martin, Z. Hao, H. A. Bechtel, X. Liang, A. Zettl, Y. R. Shen, and F. Wang, Nature Nanotech. **6**, 630 (2011).
[20] A. Yu. Nikitin, F. Guinea, F. J. Garcia-Vidal, and L. Martin-Moreno, Phys. Rev. B **84**, 161407 (2011).
[21] S. Thongrattanasiri, F. H. L. Koppens, and F. J. Garcia de Abajo, Phys. Rev. Lett. **108**, 047401 (2012).
[22] A. Y. Nikitin, F. Guinea, F. J. Garcia-Vidal, and L. Martin-Moreno, Phys. Rev. B **85**, 081405 (2012).
[23] F. H. Koppens, D. E. Chang, and F. J. Garcia de Abajo, Nano Lett. **11**, 3370 (2011).
[24] A. Vakil and N. Engheta, Science **332**, 1291 (2011).
[25] F. Rana, IEEE Trans. Nanotechnol. **7**, 91 (2008).
[26] A. A. Dubinov, V. Y. Aleshkin, V. Mitin, T. Otsuji, and V. Ryzhii, J. Phys.: Condens. Matter **23**, 145302 (2011).
[27] A. Bostwick, T. Ohta, T. Seyller, K. Horn, and E. Rotenberg, Nature Phys. **3**, 36 (2007).
[28] V. Ryzhii, M. Ryzhii, V. Mitin, A. Satou, and T. Otsuji, Jpn. J. Appl. Phys. **50**, 094001 (2011).
[29] L. A. Falkovsky and S. S. Pershoguba, Phys. Rev. B **76**, 153410 (2007).
[30] N. M. R. Peres, Rev. Mod. Phys. **82**, 2673 (2010).
[31] Y.-W. Tan, Y. Zhang, K. Bolotin, Y. Zhao, S. Adam, E. H. Hwang, S. Das Sarma, H. L. Stormer, and P. Kim, Phys. Rev. Lett. **99**, 246803 (2007).
[32] M. Orlita, C. Faugeras, P. Plochocka, P. Neugebauer, G. Martinez, D. K. Maude, A.-L. Barra, M. Sprinkle, C. Berger, W. A. de Heer, and M. Potemski, Phys. Rev. Lett. **101**, 267601 (2008).
[33] M. Sprinkle, D. Siegel, Y. Hu, J. Hicks, A. Tejeda, A. Taleb-Ibrahimi, P. Le Fevre, F. Bertran, S. Vizzini, H. Enriquez, S. Chiang, P. Soukiassian, C. Berger, W. A. de Heer, A. Lanzara, and E. H. Conrad, Phys. Rev. Lett. **103**, 226803 (2009).

[34]J. M. Dawlaty, S. Shivaraman, M. Chandrashekhar, F. Rana, and M. G. Spencer, Appl. Phys. Lett. **92**, 042116 (2008).
[35]T. Otsuji, S. A. Boubanga Tombet, A. Satou, H. Fukidome, M. Suemitsu, E. Sano, V. Popov, M. Ryzhii, and V. Ryzhii, J. Phys. D: Appl. Phys. **45**, 303001 (2012).
[36]V. Ryzhii, M. Ryzhii, A. Satou, T. Otsuji, A. A. Dubinov, and V. Y. Aleshkin, J. Appl. Phys. **106**, 084507 (2009).
[37]F. Rana, Phys. Rev. B **76**, 155431 (2007).
[38]R. Kim, V. Perebeinos, and P. Avouris, Phys. Rev. B **84**, 075449 (2011).
[39]T. Winzer and E. Malić, Phys. Rev. B **85**, 241404(R) (2012).
[40]D. V. Fateev, V. V. Popov, and M. S. Shur, Fiz. Tekh. Poluprovodn. **44**, 1455 (2010) [Semiconductors **44**, 1406 (2010)].
[41]See Supplemental Material at http://link.aps.org/supplemental/10.1103/PhysRevB.86.195437 for more details of our theoretical approach.
[42]V. V. Popov, A. N. Koudymov, M. Shur, and O. V. Polischuk, J. Appl. Phys. **104**, 024508 (2008).
[43]V. V. Popov, G. M. Tsymbalov, D. V. Fateev, and M. S. Shur, Appl. Phys. Lett. **89**, 123504 (2006).
[44]V. V. Popov, O. V. Polischuk, T. V. Teperik, X. G. Peralta, S. J. Allen, N. J. M. Horing, and M. C. Wanke, J. Appl. Phys. **94**, 3556 (2003).
[45]V. V. Popov, D. V. Fateev, O. V. Polischuk, and M. S. Shur, Opt. Express **18**, 16771 (2010).
[46]B. Luk'yanchuk, N. I. Zheludev, S. A. Maier, N. J. Halas, P. Nordlander, H. Giessen, and T. C. Chong, Nat. Mater. **9**, 707 (2010).
[47]A. E. Miroshnichenko, S. Flach, and Y. S. Kivshar, Rev. Mod. Phys. **82**, 2257 (2010).
[48]M. G. Benedict, A. M. Ermolaev, V. A. Malyshev, I. V. Sokolov, and E. D. Trifinov, *Superradiance: Multiatomic Coherent Emission* (IOP, Bristol, 1996).
[49]Y. Sonnefraud, N. Verellen, H. Sobhani, G. A. E. Vandenbosch, V. V. Moshchalkov, P. Van Dorpe, P. Nordlander, and S. A. Maier, ACS Nano **4**, 1664 (2010).
[50]E. M. Purcell, Phys. Rev. **69**, 681 (1946).